University of Texas Rio Grande Valley

ScholarWorks @ UTRGV

Chemistry Faculty Publications and Presentations

College of Sciences

5-1-2015

TiO 2 Fibers: Tunable Polymorphic Phase Transformation and Electrochemical Properties

Edna Garcia
The University of Texas Rio Grande Valley

Qiang Li
The University of Texas Rio Grande Valley

Xing Sun
The University of Texas Rio Grande Valley

Karen Lozano
The University of Texas Rio Grande Valley, karen.lozano@utrgv.edu

Yuanbing Mao
The University of Texas Rio Grande Valley, yuanbing.mao@utrgv.edu

Follow this and additional works at: https://scholarworks.utrgv.edu/chem_fac

Part of the Chemistry Commons, and the Nanoscience and Nanotechnology Commons

TiO$_2$ Fibers: Tunable Polymorphic Phase Transformation and Electrochemical Properties

Edna Garcia[1, †], Qiang Li[1, 2, †], Xing Sun[1], Karen Lozano[2], and Yuanbing Mao[1, *]

[1]*Department of Chemistry, University of Texas-Pan American, Edinburg, TX 78539, USA*
[2]*Department of Mechanical Engineering, University of Texas-Pan American, Edinburg, TX 78539, USA*

A series of one-dimensional (1D) nanoparticle-assembled TiO$_2$ fibers with tunable polymorphs were prepared via a novel and large scale ForceSpinning® process of titanium tetraisopropoxide (TTIP)/polyvinylpyrrolidone (PVP) precursor fibers followed with a thermal treatment at various calcination temperatures. The thermal and structural transformations were characterized by thermogravimetric analysis/differential scanning calorimetry, scanning electron microscopy, and X-ray diffraction. The influence of polymorphic phase of the TiO$_2$ fibers on the electrochemical performance in neutral aqueous 1 M Na$_2$SO$_4$ electrolyte was investigated. The polymorphic amorphous/anatase/rutile TiO$_2$ fibers prepared at 450 °C achieved a highest capacitance of 21.2 F g^{-1} (6.61 mF cm^{-2}) at a current density of 200 mA g^{-1}, for which the improved electronic conductivity and activated pseudo-capacitance mechanism may be responsible. This work helps bridge the gap between nanoscience and manufacturing. It also makes polymorphism control of functional materials a potential strategy for further improving supercapacitive output of metal oxides.

Keywords: ForceSpinning, TiO$_2$, Fibers, Polymorphism, Energy Storage.

1. INTRODUCTION

As a wide-band gap semiconductor, titanium dioxide (TiO$_2$) has been exploited in a myriad of aspects, such as photocatalysis, gas sensors, waste remediation, electrochromics, photovoltaic solar cells, electrochemical energy storage devices and drug delivery with its advantages over other materials, including earth abundance, non-toxicity, chemical stability and photochemical/electrochemical activity.[1–8] Along with the urgent demands of developing new green electric vehicles and grid storage devices to substitute fossil fuel-based counterparts, the advantageous TiO$_2$ has been ushered into electrochemical energy storage devices through various routes:[9–14] nanostructured to increase the accessible electroactive sites and shorten the ionic diffusion paths; hydrogenated to improve capacitive performance by forming oxygen vacancies (Ti^{3+} sites);[9] to accommodate one Li$^+$ ion per Ti into amorphous and bronze-type TiO$_2$ nanostructures as an anode material of lithium-ion

batteries;[10, 11] to use the size effect (< 30 nm) to increase the pseudocapacitance contribution to overall energy storage performance;[12] and to employ fine TiO$_2$ nanoarchitectures as templates to carry electroactive Faradic redox oxides for enhanced electrode materials.[13] However, TiO$_2$ has still not been used satisfactorily as a supercapacitive material because its capacitances only range from 40 nF cm^{-2} to 3.24 mF cm^{-2} as previously reported in the literature.[9, 15] Moreover, an industrially valuable synthetic protocol which is cost-effective and scalable has to be developed yet.

The TiO$_2$ polymorphs comprise connected octahedra where Ti occupies the center and oxygen at every vertex. Differently ordered TiO$_6$ octahedra form distinct unit cells such as anatase, rutile and brookite phases. Its polymorphic combinations can result in different characteristics and properties.[16–19] For instance, the polymorphic mixture of 70% anatase and 30% rutile was found to have enhanced photocatalytic activity due to the reduced recombination of photogenerated electrons and holes and the formation of semiconductor–semiconductor junction.[16] However, to the best knowledge of the authors, there

is only one report in the literature studied the influence of polymorphic coexistence of TiO_2 on conventional electric double-layer capacitance and/or subsurface pseudocapacitance. In 2012, Salari et al. reported that biphasic anatase/rutile nanotube arrays prepared anodically could deliver a relative high areal capacitance of 2.6 mF cm^{-2},[17] even though it is difficult to scale up the fabrication process for these TiO_2 nanotube arrays, and so to further improve their areal electrochemical performance. Meanwhile, the low fabrication efficiency of the tedious anodical process contradicts the requirement of efficient manufacture to satisfy the application needs.

Here we demonstrated a novel ForceSpinning® (FS) method to fabricate titanium (IV) tetraisopropoxide (TTIP)/polyvinylpirrolidone (PVP) composite microfibers with high throughput. As a high-yield manufacturing technique for fine fibers, the throughput on a laboratory scale setup is larger than 1 g min^{-1}.[20] Subsequent calcination at varying temperatures partially or completely removes the sacrificial while heavily-loaded "carrier polymer" PVP to generate uniform fibers consisting of fine TiO_2 nanoparticles. During the calcination process, the polymorphic composition of TiO_2 phases can be well controlled by the calcination temperature. In this study, the influence of calcination temperature on polymorphic transforms from the titanium precursor to TiO_2 and the effect of TiO_2 polymorphs on electrochemical performance were also studied. An uncommon phase transition profile with calcination temperature was found in this study. Moreover, a highest capacitance of 21.2 F g^{-1} (6.61 mF cm^{-2}) was achieved for the first time from our TiO_2 fibers with an amorphous/anatase/rutile polymorph after calcined at 450 °C.

2. EXPERIMENTAL DETAILS
2.1. Preparation of TiO₂ Fibers
Precursor solution for the FS process was prepared by dissolving 1.5 g of PVP (MW = 1,300,000, Aldrich) into a mixture of 9 mL of ethanol and 3 mL of acetic acid under vigorous stirring for 3 h. Subsequently, 0.75 mL of TTIP (99.99%, Aldrich) was quickly added into above mixture. The mixture was then magnetically stirred for approximately 1 h, allowed to degas for 3 h to remove any trapped air-bubbles, and spun by a proprietary FS apparatus equipped with a spinneret (with 8 equally circumferentially spaced orifices) at 9000 rpm with an 6 cm orifice-to-collector distance. The as-spun precursor fibers were calcined at different temperatures of 400, 450, 500, 550, 600, and 650 °C in air for 3 h at a ramp rate of 5 °C min^{-1} to generate the TiO_2 fibers. Depending on the calcination temperatures, these fibers are designated as TF400, TF450, TF500, TF550, TF600 and TF650, respectively.

2.2. Characterizations
The morphological, structural and compositional information of the resultant fibers before and after calcining the TTIP/PVP precursor microfibers were characterized using a Zeiss Sigma VP field emission scanning electron microscopy (SEM) equipped with a back-scatter detector, a Bruker AXS D8 QUEST X-ray diffraction (XRD), a TA Instrument Q500 thermogravimetric analysis (TGA) and Q20 differential scanning calorimetry (DSC).

2.3. Electrochemical Evaluations
Cyclic voltammetry (CV), galvanostatic charge/discharge measurements and electrical impedance spectroscopy (EIS) conducted in the frequency range of 1 MHz to 10 mHz were performed for calcined TiO_2 fiber-coated working electrodes in a three-electrode cell using a Potentiostat/Galvanostat/ZRA (Gamry Reference 600) Electrochemical Workstation. 1 M Na_2SO_4 aqueous solution was employed as the electrolyte, a platinum wire as the counter electrode, and an Ag/AgCl electrode as the reference. The working electrodes were fabricated as below: the calcined TiO_2 fibers were first evenly grinded with carbon black and polyvinylidene fluoride (PVDF) with a weight ratio of 80:10:10 in dimethyl formamide (DMF). The formed slurry was pasted onto a graphite fiber-based current collector. And then the prepared working electrodes were thoroughly dried at 60 °C overnight in a vacuum oven before electrochemical testing.

3. RESULTS AND DISCUSSION
The FS process, as schematically shown in Figure 1(a), successfully produced the TTIP/PVP precursor microfibers. In principle, during the FS process, high-speed rotation drives viscous precursor solutions out of the spinning reservoir through spinneret orifices to form fibers once centrifugal force and hydrostatic pressure exceeded capillary force. SEM image shown in Figure 1(b) demonstrates a non-woven network composed of the randomly oriented TTIP/PVP precursor fibers. The as-spun fibers have smooth surface without beads-on-string phenomenon. The average diameter of these fibers is about 2 μm. The back-scattered SEM image with smooth contrast indicates that the titanium precursor disperses uniformly in these microfibers. Noteworthy is that the high-throughput FS process yields fine fibers with no need of adjusting complicated parameters. The only vital factors of the FS process are solution viscosity and orifice-to-collector distance.[20]

Figure 2 shows the thermal analyses on the TTIP/PVP fibers. On the TGA thermogram, the 62% mass lose in the temperature range of 300 to 455 °C correlates with the two broad exothermic peaks at 327 °C and 410 °C on the DSC thermogram. This two-step degradation relates to the breakage of pyrrolidone pendant groups off the
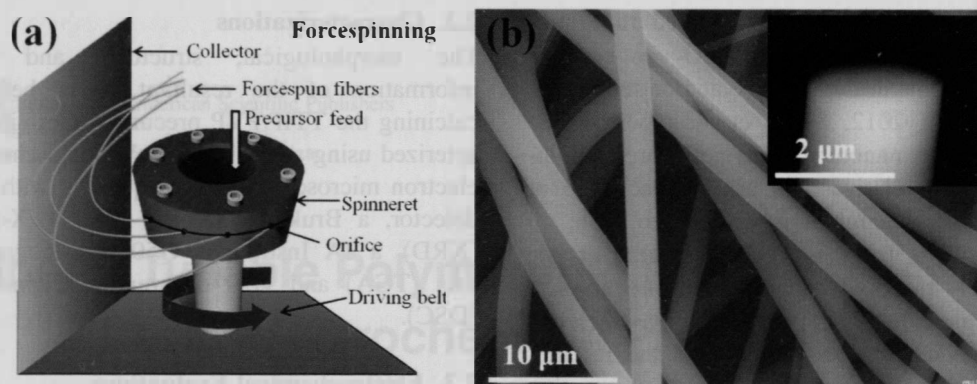
Figure 1. (a) Schematic representation of the ForceSpinning process. (b) SEM image of the as-spun TTIP/PVP precursor fibers taken under environmental conditions. Inset in panel (b) is a back-scattered SEM image taken from the end of an individual precursor fiber.

PVP backbone and the subsequent breaking down of the main hydrocarbon chain. The sharp exothermic peak at 297 °C on the DSC thermogram represents the pyrolysis of non-hydrolyzed titanium precursor TTIP. The exothermic peak located at 475 °C is attributed to the crystallization of rutile phase from anatase phase while the crystallization peaks from amorphous to anatase and rutile phases presumably overlaps with the broad PVP degradation peak.[21]

Figure 3 shows the morphology of the TiO$_2$ fibers obtained after calcining the TTIP/PVP microfibers at temperatures between 400 to 650 °C. It can be clearly observed that the TTIP/PVP microfibers underwent significant shrinkage due to the removal of the heavily-loaded "polymer carrier" PVP (partial or complete removal depending on the calcinations temperature and duration). The diameter of the TiO$_2$ fibers is in the range of 500 nm to 1 μm. The insets with SEM images taken at higher magnification confirm that these fibers were packed with quite uniform TiO$_2$ nanoparticles. The particle size from these fibers increases evidently with
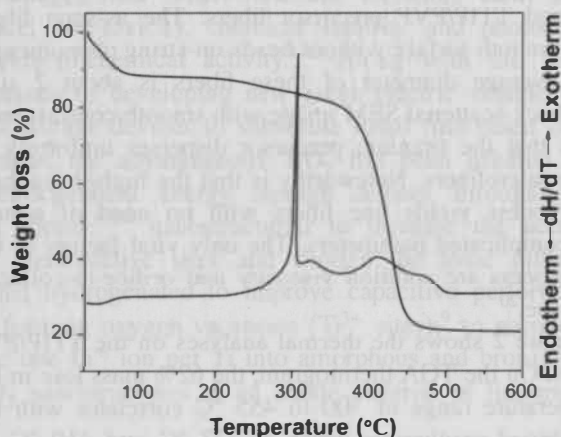

Figure 2. TGA/DSC thermograms of the as-spun TTIP/PVP precursor fibers.

the increasing calcination temperature from 400 °C to 650 °C.

The influence of calcination temperature on polymorphic transforms from the titanium precursor to TiO$_2$ was studied by XRD. The XRD patterns in Figure 4 demonstrate that TF400 presents the anatase TiO$_2$ crystalline structure only (JCPDS #89-4921). When calcination temperature was equal to or greater than 450 °C, rutile phase of TiO$_2$ (JCPDS #21-1276) was also identified.[18, 19, 22] As shown in Table I, when the calcination temperature increased from 400 °C to 650 °C, the crystalline size calculated by the Debye-Scherrer equation increased from 7 nm to 30 nm, consistent with the SEM observation shown in Figure 3. Without considering the coexistence of amorphous phase in the TiO$_2$ fibers, the composition ratio of anatase to rutile phases was calculated using the following formula:

$$W_R = \frac{A_R}{0.886A_A + A_R} \tag{1}$$

where W_R is the weight fraction of the rutile phase, A_A and A_R denote the anatase (101) and rutile (110) reflection intensity, respectively.[16] Noted is that W_R from our TiO$_2$ fibers does not always increase with increasing calcination temperature, unlike reported observations in the literature.[16, 23, 24] The TF450 sample contained about 72 wt.% rutile phase, which is anomaly high, over 28 wt.% of anatase after the precursor fibers were only calcined at 450 °C. Here we postulated that amorphous, anatase and rutile phases co-exist in the TF450 sample, and the rutile phase was derived directly from the amorphous precursor after calcined at 450 °C based on our reproducible observation and the following factors: (1) the amorphous phase consists of rich superficial defects including TiO$_6$ and TiO$_5$ complexes, which resemble octahedra organization of the rutile phase. Therefore, when calcined at 450 °C, the provided thermal energy is high enough to make the amorphous-to-rutile transformation possible, and the amorphous TiO$_2$ converted directly to rutile phase easily. (2) In comparison with common sol–gel and
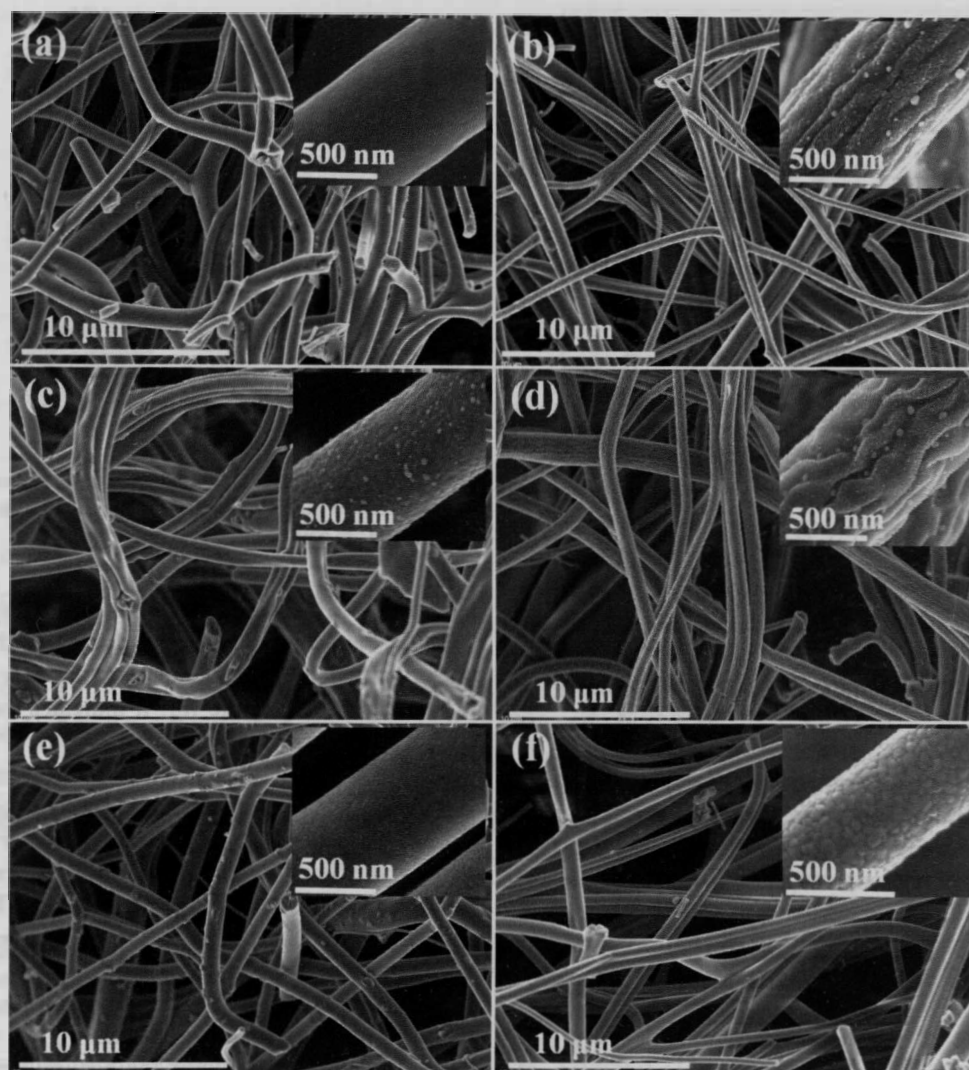
3752

Figure 3. (a)–(f) SEM images of the TiO$_2$ fibers obtained after calcining the TTIP/PVP microfibers at 400 °C, 450 °C, 500 °C, 550 °C, 600 °C and 650 °C, respectively. The insets show the corresponding SEM images taken at high magnifications.

electrospinning processes, our FS process applies much heavily-loaded "carrier polymer" PVP. The excess polymer is expected to affect the calcinations process, and therefore the crystallization process of TiO$_2$. This gave the TF450 sample a unique amorphous/anatase/rutile composite characteristic with relatively high ratio of rutile to anatase phase. When the calcination temperature is high enough, e.g., at 500 °C, the carrier polymer is completely burned off, and the crystallization process of TiO$_2$ turns back into normal. More specifically, the amorphous titanium oxide precursor would convert into anatase phase more easily than rutile phases, which causes the relatively decreased rutile-to-anatase ratio compared to the sample calcined at 450 °C. The actual amount of anatase and rutile phases should be higher at 500 °C than at 450 °C though. With the temperature was further increased to greater than 500 °C, more and more anatase nanocrystals convert into rutile phase upon temperature fulfilling the activation energy, and the rutile phase became gradually dominant over the

anatase phase. To sum, the phase transformation of the TiO$_2$ fibers from our TTIP/PVP microfibers via calcinations is illustrated in Scheme 1. However, the unprecedented phase transformation of titanium oxide observed in this study needs separate detailed investigation in the future.

The effect of TiO$_2$ polymorphs on electrochemical performance was further studied. First, the CV measurements (Figs. 5(A) and (B)) were carried out at potentials of 0–0.7 V to investigate the influence of phase combinations on capacitive performance. The quasi-rectangular CV profiles imply a nearly ideal supercapacitive performance. Base on the comparative CV curves at a scan rate of 100 mV s^{-1}, the integrated area suggests the amorphous/anatase/rutile TF450 sample has the largest gravimetric capacitance and a significant decline in capacitance occurs as the rutile content increases. The specific capacitance (Table I) is calculated from the galvanostatic
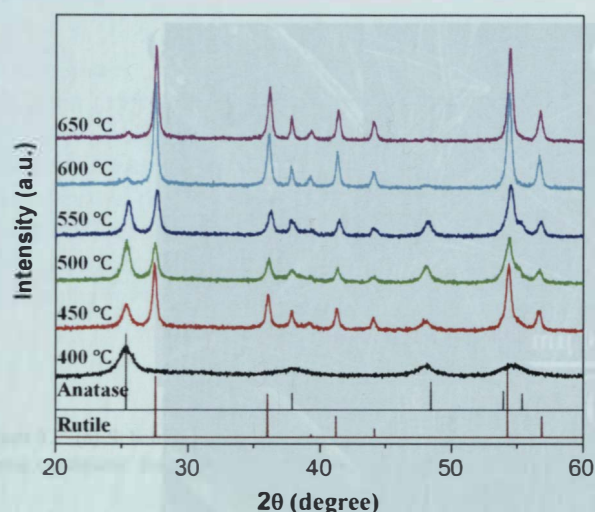
Figure 4. XRD patterns of the TiO₂ fibers obtained after calcining the TTIP/PVP microfibers at 400 °C, 450 °C, 500 °C, 550 °C, 600 °C and 650 °C, respectively. The JCPDS files of the anatase (#89-4921) and rutile (#21-1276) phases of TiO₂ are also shown for comparison.

Scheme 1. The schematic illustration of the phase transformation of the TiO₂ fibers from our TTIP/PVP microfibers after calcined at temperatures from 400 °C to 650 °C.

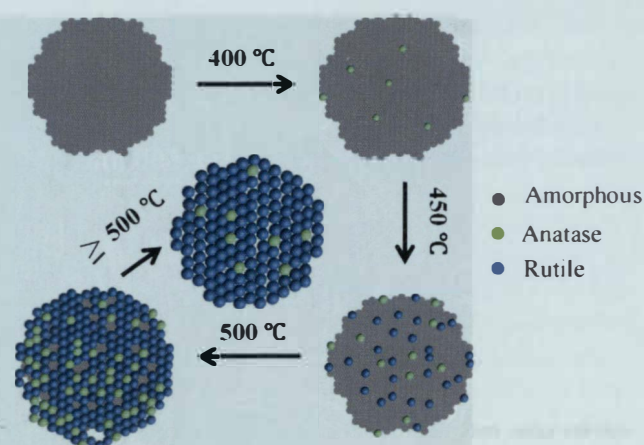charge/discharge studies (Figs. 5(C) and (D)) following the formula below:

$$C_S = \frac{I \times t}{\Delta V \times m} \tag{2}$$

where C_s is the specific capacitance (F g⁻¹), m is the active material mass (g), I and t are the discharge current (A) and the discharge time (second), respectively, in the potential range ΔV excluding the IR drop. The TF450 delivers the highest capacitance of 21.2 F g⁻¹ (6.61 F cm⁻²) at a current density of 200 mA g⁻¹, which is higher than the previously reported results (< 3.24 mF cm⁻² or 2.6 mF cm⁻² from Refs. [9 and 17], respectively). The non-woven mat of the TiO₂ fibers does not punish the rate capacity and capacitive performance because electrolyte ions can easily percolate into the network of our TiO₂ fibers. Another advantage here is that our FS method can be readily scaled up for making one-dimensional mixed-phase TiO₂ fibers.

Figure 6 shows the EIS data which is also fitted by the equivalent circuit diagram. The intercept at real axis representing the internal combined resistance (R_s), the compressed semicircle in the high-to-medium frequency area associated with the charge transfer resistance (R_{ct}),

and a slope line at low frequency corresponding to the Warburg impedance (Z_w). Compared to the TF550 sample, the TF450 electrode shows a smaller R_s (2.4 Ω vs. 6.2 Ω) and a negligible R_{ct}. It indicates the advantageous TF450 electrode has a superior electrical contact among fibers and on electrode/current collector interface. It also possesses a favorable electronic transportation. While the TF550 electrode exhibits a relatively vertical line leaning to the imaginary axis at the low frequency region implying an ideal capacitive behavior, the TF450 electrode shows a more inclined line suggesting a pseudocapacitive feature.[25]

The unique FS process requires heavy polymer loadings as spinning media to create highly viscous precursor solutions. In this study, the heavily loaded PVP acted as a framework to prevent further quick growth of the amorphous TiO₂ and derivative anatase and rutile nanoparticles upon hydrolysis and pyrolysis. These nanoscaled TiO₂ particles may possess a great number of TiO₅ complexes on the surface, which generates increased oxygen vacancies known as the electron donors for TiO₂.[26] The formation of vacancies (Ti³⁺ sites) may activate the pseudocapacitive storage mechanism. Simultaneously, the ∼10 nm nanoparticles, especially in the TF450 sample, significantly shorten the ionic diffusion paths. In addition, the improved electronic conductivity due to the polymorphic coexistence and the increased surface area of our TiO₂ fibers enhance the electric double-layer capacitance as well. These characteristics may account for the greatly enhanced electrochemical performance of the TF450 sample. In other words, the decrease of disordered amorphous and anatase phases upon increasing the calcination temperature as well as the grain growth decreases the electrochemical performance of the TF500–650 samples. Our future endeavor will be to continue downsizing these TiO₂ fibers, to further investigate the anomaly phase transformation process during the calcination of the TTIP/PVP
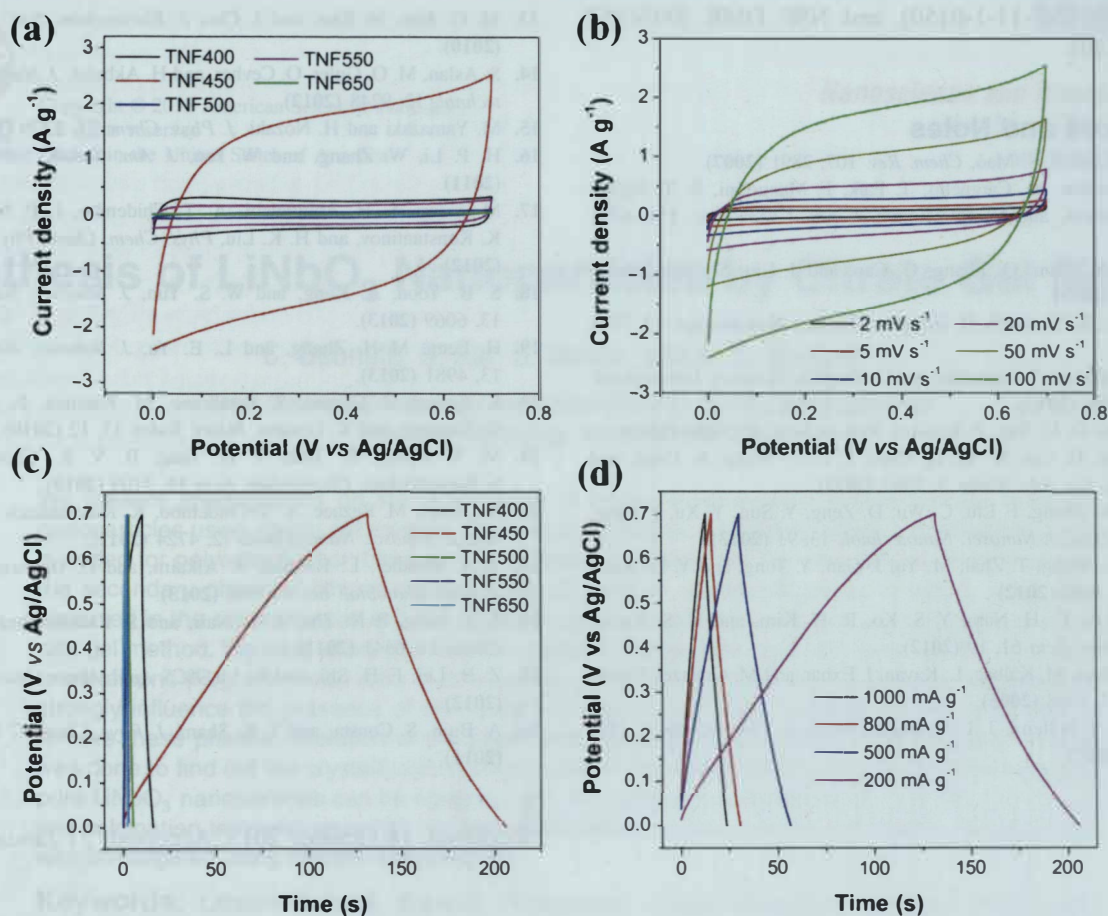
Table I. Structural, crystalline and electrochemical characteristics of the TiO₂ fibers obtained after calcining the TTIP/PVP microfibers at 400 °C, 450 °C, 500 °C, 550 °C, 600 °C and 650 °C, respectively.

Sample	Particle size (nm)	Rutile/Anatase weight ratio	Specific capacitance (F g⁻¹)
TNF400	7.2	0/100	1.65
TNF450	11.5	72/28	21.2 (6.61 F cm⁻²)
TNF500	15.0	54/46	0.34
TNF550	23.8	60.5/39.5	0.10
TNF600	29.1	86.6/13.4	—
TNF650	30.3	87/13	0.0076

Figure 5. Electrochemical properties of the TiO₂ fibers. CV curves of (A) the TF400–650 samples at a scan rate of 100 mV s⁻¹ and (B) the TF450 at various scan rates. Galvanostaic charge/discharge measurements of (C) the TF400–650 at a current density of 200 mA g⁻¹ and (D) the TF450 at various current densities.

precursor fibers, and to understand the underlying mechanism related to the high electrochemical performance of the TiO₂ fibers prepared by the FS method, especially the amorphous/anatase/rutile polymorphic sample.
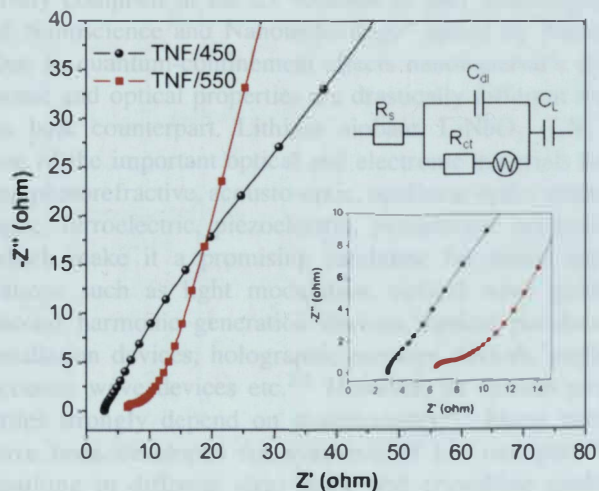

Figure 6. EIS spectra of the typical TF450 and TF550 samples with the insets showing the high-frequency region and the equivalent circuit diagram used to fit the EIS spectra.

4. CONCLUSION

Precursor TTIP/PVP microfibers were successfully prepared using a novel ForceSpinning process with simplicity and high throughput. Calcination temperature was varied to generate TiO₂ fibers with different polymorphic mixture. Very interestingly, after calcining the precursor fibers at 450 °C, the obtained TF450 sample contains anomaly high ratio of rutile phase to anatase phase ∼72 wt.% to 28 wt.%. More importantly, the influence of these tunable phase transformations on electrochemical performance was evaluated. The TiO₂ fibers prepared at a calcination temperature of 450 °C exhibited a unique amorphous/anatase/rutile polymorph. They demonstrated a highest capacitance of 21.2 F g⁻¹ (6.61 mF cm⁻²) for TiO₂ at a current density of 200 mA g⁻¹, which surpasses previously reported results. Therefore, polymorphic control of electrode materials can be a promising strategy to improve their electrochemical performance.

References and Notes

1. X. Chen and S. S. Mao, *Chem. Rev.* 107, 2891 (2007).
2. T. R. Gordon, M. Cargnello, T. Paik, F. Mangolini, R. T. Weber, P. Fornasiero, and C. B. Murray, *J. Am. Chem. Soc.* 134, 6751 (2012).
3. Z. Nie, X. Zhou, Q. Zhang, G. Cao, and J. Liu, *Sci. Adv. Mater.* 5, 1750 (2013).
4. H. H. Ko, S. Yi, and S. H. Jeong, *J. Nanosci. Nanotechnol.* 13, 7906 (2013).
5. M. V. Sofianou, T. Vaimakis, and C. Trapalis, *Nanosci. Nanotechnol. Lett.* 5, 461 (2013).
6. S. Xu and D. D. Sun, *J. Nanosci. Nanotechnol.* 13, 6866 (2013).
7. X. Cheng, H. Liu, X. Yu, Q. Chen, J. Li, P. Wang, A. Umar, and Q. Wang, *Sci. Adv. Mater.* 5, 1563 (2013).
8. S. Lai, W. Zhang, F. Liu, C. Wu, D. Zeng, Y. Sun, Y. Xu, Y. Fang, and W. Zhou, *J. Nanosci. Nanotechnol.* 13, 91 (2013).
9. X. Lu, G. Wang, T. Zhai, M. Yu, J. Gan, Y. Tong, and Y. Li, *Nano Lett.* 12, 1690 (2012).
10. W. H. Ryu, D. H. Nam, Y. S. Ko, R. H. Kim, and H. S. Kwon, *Electrochim. Acta* 61, 19 (2012).
11. M. Zukalova, M. Kalbac, L. Kavan, I. Exnar, and M. Graetzel, *Chem. Mater.* 17, 1248 (2005).
12. J. Wang, J. Polleux, J. Lim, and B. Dunn, *J. Phys. Chem. C* 111, 14925 (2007).
13. M. G. Kim, H. Kim, and J. Cho, *J. Electrochem. Soc.* 157, A802 (2010).
14. S. Aslan, M. O. Guler, O. Cevher, and H. Akbulut, *J. Nanosci. Nanotechnol.* 12, 9248 (2012).
15. M. Yamazaki and H. Nozaki, *J. Phys. Chem.* 75, 1279 (1971).
16. H. P. Li, W. Zhang, and W. Pan, *J. Am. Ceram. Soc.* 94, 3184 (2011).
17. M. Salari, S. H. Aboutalebi, A. T. Chidembo, I. P. Nevirkovets, K. Konstantinov, and H. K. Liu, *Phys. Chem. Chem. Phys.* 14, 4770 (2012).
18. S. B. Yoon, A. Kang, and W. S. Yun, *J. Nanosci. Nanotechnol.* 13, 6069 (2013).
19. H. Feng, M.-H. Zhang, and L. E. Yu, *J. Nanosci. Nanotechnol.* 13, 4981 (2013).
20. K. Sarkar, C. Gomez, S. Zambrano, M. Ramirez, E. de Hoyos, H. Vasquez, and K. Lozano, *Mater. Today* 13, 12 (2010).
21. M. V. Reddy, R. Jose, T. H. Teng, B. V. R. Chowdari, and S. Ramakrishna, *Electrochim. Acta* 55, 3109 (2010).
22. M. Salari, M. Rezaee, A. T. Chidembo, K. Konstantinov, and H. K. Liu, *J. Nanosci. Nanotechnol.* 12, 4724 (2012).
23. T. A. Kandiel, L. Robben, A. Alkaim, and D. Bahnemann, *Photochem. Photobiol. Sci.* 12, 602 (2013).
24. S. Y. Yang, P. N. Zhu, A. S. Nair, and S. Ramakrishna, *J. Mater. Chem.* 21, 6541 (2011).
25. Z. B. Lei, F. H. Shi, and L. Lu, *ACS Appl. Mater. Interf.* 4, 1058 (2012).
26. A. Buin, S. Consta, and T. K. Sham, *J. Phys. Chem. C* 115, 22257 (2011).